

12

FB

AD A 023898

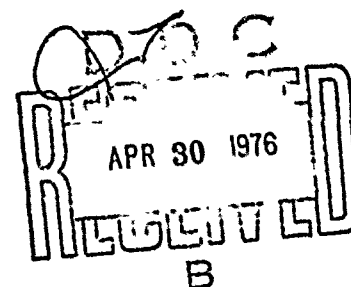
Graphite Ablation Chemistry Nonequilibrium Effects

R. L. BAKER
Vehicle Engineering Division
Engineering Science Operations
The Aerospace Corporation
El Segundo, Calif. 90245

22 March 1976

Final Report

APPROVED FOR PUBLIC RELEASE:
DISTRIBUTION UNLIMITED

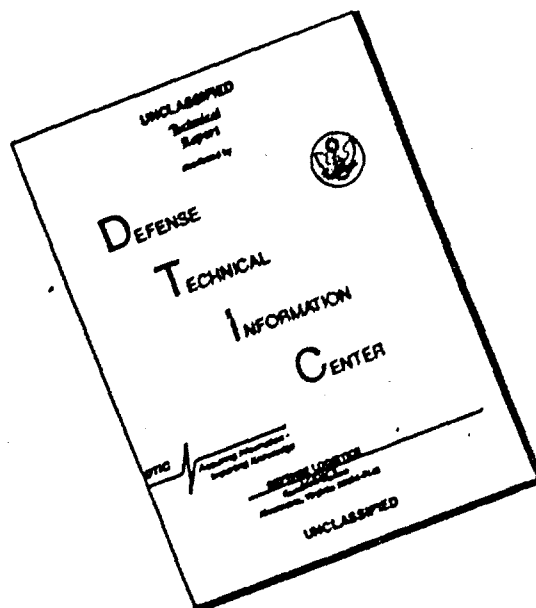


Prepared for
SPACE AND MISSILE SYSTEMS ORGANIZATION
AIR FORCE SYSTEMS COMMAND
Los Angeles Air Force Station
Los Angeles, Calif. 90045



THE AEROSPACE CORPORATION

DISCLAIMER NOTICE



THIS DOCUMENT IS BEST QUALITY AVAILABLE. THE COPY FURNISHED TO DTIC CONTAINED A SIGNIFICANT NUMBER OF PAGES WHICH DO NOT REPRODUCE LEGIBLY.

This report was submitted by The Aerospace Corporation, El Segundo CA 90245, under Contract F04701-75-C-0076 with the Space and Missile Systems Organization, Deputy for Reentry Systems, P. O. Box 92960, Worldway Postal Center, Los Angeles CA 90009. It was reviewed and approved for The Aerospace Corporation by E. G. Hertler, Vehicle Engineering Division and R. G. Allen, Reentry Systems Division. Lt. Edward Taylor, SAMSO/RSSE, was the project officer.

This technical report has been reviewed and is approved for publication. Publication of this report does not constitute Air Force approval of the report's findings or conclusions. It is published only for the exchange and stimulation of ideas.

This report has been reviewed by the Information Office (OI) and is releasable to the National Technical Information Service (NTIS). At NTIS, it will be available to the general public, including foreign nations.

Edward G. Taylor
Edward G. Taylor, 1st Lt, USAF
Aeromechanics & Materials Division
Directorate of Ballistic Systems
Deputy for Reentry Systems

Donald A. Dowler
Donald A. Dowler, Col, USAF
Director, Ballistic Systems
Deputy for Reentry Systems

FOR THE COMMANDER

Richard K. Saxer
Richard K. Saxer
Colonel, USAF
Deputy for Reentry Systems

✓

| | |
|--------------|---|
| NTIS | ✓ |
| DDC | |
| USMA | |
| JUSTICE | |
| BY | |
| DISTRIBUTION | |
| DISC. | |

SECURITY CLASSIFICATION OF THIS PAGE (When Data Entered)

DD FORM 1473
1EACSIMILE


SECURITY CLASSIFICATION OF THIS PAGE (When Data Entered)

UNCLASSIFIED

SECURITY CLASSIFICATION OF THIS PAGE(When Data Entered)

19. KEY WORDS (Continued)

20. ABSTRACT (Continued)

Calculations made to determine the convective heat flux required to reach an incipient melt temperature of 3800°K indicate that the required flux determined from an equilibrium calculation can be too high by as much as 200-300 percent for stagnation enthalpies less than 5000 Btu/lb. Calculations for superorbital reentry conditions show large differences in the mass addition parameter B' when the convective heating rate is low and the external radiation heating level is relatively high. Similar large differences in B' could be simulated in an existing ground test facility if the reported external radiation heating level could be increased. Such an experiment would provide data to test the validity of present convective heating rate blowing corrections in a combined heating environment. 

UNCLASSIFIED

SECURITY CLASSIFICATION OF THIS PAGE(When Data Entered)

CONTENTS

| | |
|---|---|
| ABSTRACT | 1 |
| INTRODUCTION | 1 |
| PROBLEM FORMULATION | 1 |
| The Knudsen-Langmuir Equation | 1 |
| Mass Conservation Equation - Binary System | 1 |
| Mass Conservation Equation - Multiple Species | 2 |
| Energy Conservation Equation | 3 |
| Primary Dependent and Independent Variables | 3 |
| DISCUSSION OF RESULTS | 4 |
| The Nature of Nonequilibrium Effects | 4 |
| Graphical Solution Procedure | 4 |
| Mass Loss and Surface Temperature Differences for Typical Reentry Vehicle Environments | 5 |
| Graphite Melt Considerations | 5 |
| Radiation Heating Effects. | 6 |
| SUMMARY AND CONCLUSIONS | 7 |
| APPENDIX: THERMOCHEMISTRY DATA | 7 |
| REFERENCES | 8 |

FIGURES

| | | |
|----|---|---|
| 1. | Microscopic Surface Mass Balance | 2 |
| 2. | Macroscopic Surface Mass Balance | 2 |
| 3. | Macroscopic Surface Energy Balance | 3 |
| 4. | Differences Between Equilibrium and Nonequilibrium Solutions | 4 |
| 5. | Nonequilibrium Effects on B' and T_w | 5 |
| 6. | Nonequilibrium Effect on Surface Recession Rate | 5 |
| 7. | Nonequilibrium Effect on Surface Temperature | 5 |
| 8. | Nonequilibrium Effects on Melt Temperature Environments | 6 |

TABLES

| | | |
|----|---|---|
| 1. | Equilibrium B' Values | 4 |
| 2. | Superorbital Reentry Calculations | 7 |
| 3. | Large B' in a Ground Test Environment | 7 |

GRAPHITE ABLATION CHEMISTRY NONEQUILIBRIUM EFFECTS*

R. L. Baker**
The Aerospace Corporation
Los Angeles, California

Abstract

The implications of the assumption of local solid-gas phase equilibrium for subliming carbon species for graphite ablation calculations in an air environment is investigated. The equilibrium assumption is eliminated by considering the Knudsen-Langmuir equation at the interface for each carbon specie. Calculated equilibrium and nonequilibrium results are compared for a very wide range of flight and ground test environments. The nonequilibrium mass addition parameter is always less than the equilibrium value and the nonequilibrium wall temperature is always larger for a given environment. Calculations made to determine the convective heat flux required to reach an incipient melt temperature of 3800°K indicate that the required flux determined from an equilibrium calculation can be too high by as much as 200-300 percent for stagnation enthalpies less than 5000 Btu/lb. Calculations for superorbital reentry conditions show large differences in the mass addition parameter B' when the convective heating rate is low and the external radiation heating level is relatively high. Similar large differences in B' could be simulated in an existing ground test facility if the reported external radiation heating level could be increased. Such an experiment would provide data to test the validity of present convective heating rate blowing corrections in a combined heating environment.

Introduction

In the formulation of problems involving interphase transfer of mass, it is necessary to relate the concentrations of the principle mass transfer species in one phase to their concentrations in the other phase. For graphite ablation calculations, the carbon species concentrations in the gas phase are proportional to the partial pressures of each species at the solid-gas interface. Practically all graphite ablation calculations are made assuming that the partial pressure p_i of carbon species i at the wall is equal to the vapor pressure p_i^v of that specie at the wall temperature⁽¹⁻³⁾. In order for this to be true, the solid and the gas phase must be in equilibrium with one another at the wall temperature. If the solid and the gas phase are in equilibrium at the wall temperature, then the same number of molecules are condensing from the gas phase into the solid as those vaporizing from the solid into the gas. This means there is no net transfer of mass between phases, therefore we know the assumption that $p_i = p_i^v$ cannot be exact for finite interphase mass transfer rates.

The purpose of this work is to formulate the graphite ablation problem without making the assumption that $p_i = p_i^v$ and to determine the implications of this simplifying assumption for an air

environment by comparison of results calculated using both methods. In the remaining discussion, the problem formulation with p_i assumed equal to p_i^v at the wall temperature is simply termed equilibrium. When this assumption is not made, the term nonequilibrium formulation is used.

Problem Formulation

The Knudsen-Langmuir Equation

It can be shown from kinetic theory⁽⁴⁾ that the mass of gaseous species i striking a unit area of wall per second is given by

$$\mu_i = \sqrt{\frac{\eta_i}{2\pi RT_w}} p_i \quad (1)$$

where T_w is the wall temperature, η_i is the molecular weight of species i and p_i is the pressure. By referring to Fig. 1, we find expressions similar to that above can be written for the mass vaporizing from the liquid and condensing from the gas phase per unit area per second. Then a simple interphase mass balance gives the following expression for the net transfer of mass per unit area per second between phases

$$\dot{m}_i = \alpha_i \sqrt{\frac{\eta_i}{2\pi RT_w}} |p_i^v - p_i| \quad (2)$$

This equation is the Knudsen-Langmuir equation⁽⁴⁾. The p_i^v and p_i are the vapor pressure of species i at the wall temperature T_w , and the partial pressure of species i , one mean free path from the wall. These pressures cannot be equal to one another if there is to be any net interphase transfer of mass. The coefficient α_i in Eq. (2) is the vaporization coefficient. From kinetic theory, the maximum mass flux vaporizing per unit area of wall per second is $\sqrt{\eta_i/2\pi RT_w} p_i^v$. The actual mass flux is $\alpha_i \sqrt{\eta_i/2\pi RT_w} p_i^v$. The value of α_i must be determined experimentally⁽⁴⁾. In obtaining Eq. (2), it has been assumed that the vaporization coefficient and the condensation coefficient are equal (see Fig. 1). Equation (2) represents a surface mass balance on a microscopic or molecular level.

Mass Conservation Equation - Binary System

The principal equations used in defining the present problem are the macroscopic mass and energy conservation equations. As shown by Kubota⁽⁵⁾, modeling of the convective and diffusive mass fluxes at the wall (see Fig. 2) gives the following relationship between the mass addition parameter B' and the mass fraction of vaporizing

* This study was supported by the Air Force Space and Missile Systems Organization under Contract F04701-74-C-0075.

** Member of Technical Staff, Aerothermodynamics Department


$$\begin{aligned}\dot{m} &= \dot{m}_{\text{vap}} - \dot{m}_{\text{cond}} \\ \dot{m} &= \sqrt{\frac{\bar{m}_1}{2\pi RT_w}} [\alpha_{\text{vap}} p_1^v - \alpha_{\text{cond}} p_1] \\ \dot{m} &= \alpha_1 \sqrt{\frac{\bar{m}_1}{2\pi RT_w}} [p_1^v - p_1] \text{ FOR } \alpha_1 = \alpha_{\text{vap}} = \alpha_{\text{cond}} \\ \dot{m}_{\text{cond}} &= \alpha_{\text{cond}} \sqrt{\frac{\bar{m}_1}{2\pi RT_w}} p_1 \quad \dot{m}_{\text{vap}} = \alpha_{\text{vap}} \sqrt{\frac{\bar{m}_1}{2\pi RT_w}} p_1^v\end{aligned}$$


Fig. 1. Microscopic Surface Mass Balance

$$\begin{aligned}\dot{m} &= \dot{m}_{\text{conv}} + \dot{m}_{\text{diff}} \\ \dot{m} &= (\rho v)_w K_{1w} + \rho_e u_e C_H K_{1w} \\ \dot{m} &= \dot{m}_{K_{1w}} + \rho_e u_e C_H K_{1w} \\ B' &= \frac{\dot{m}}{\rho_e u_e C_H} = \frac{K_{1w}}{1 - K_{1w}}\end{aligned}$$


$$\dot{m}_{\text{conv}} \quad (\rho v)_w K_{1w} \quad \dot{m}_{\text{diff}} = \rho D_1 \left(\frac{\partial K_1}{\partial y} \right)_w = \rho_e u_e C_H K_{1w}$$


Fig. 2. Macroscopic Surface Mass Balance

species at the wall, K_{1w} .

$$B' = \frac{K_{1w}}{1 - K_{1w}} \quad (3)$$

K_{1w} is related to the partial pressure at the wall p_{1w} and the molecular weight \bar{m}_1 of the vaporizing specie by the relationship $K_1 = p_1 \bar{m}_1 / p_e \bar{m}$ where p_e is the pressure at the edge of the boundary layer and \bar{m} is the average molecular weight of the gas at the wall. Making this substitution into Eq. (3) and simplifying for a binary system of components 1 and 2 results in the following equation for the mass addition parameter B' :

$$B' = \frac{1}{\frac{\bar{m}_2}{\bar{m}_1} \left[\frac{p_e}{p_1} - 1 \right]} \quad (4)$$

In the equilibrium formulation, it is assumed that $p_1 = p_1^v$ leading to the well-known relationship

$$B'_{\text{eq}} = \frac{\frac{\bar{m}_1}{\bar{m}_2} \frac{p_1^v}{p_e}}{\left[1 - \frac{p_1^v}{p_e} \right]} \quad (5)$$

For the nonequilibrium formulation, the p_1 is obtained from the Knudsen-Langmuir relationship, Eq. (2). Thus, if Eqs. (2) and (3) are combined, p_1 and p_1^v are related by

$$p_1 = \frac{p_1^v}{\left[1 + \frac{\sqrt{2\pi RT_w \bar{m}_1} \rho_e u_e C_H (B'+1)}{\alpha_1 \bar{m} p_e} \right]} \quad (6)$$

where $\rho_e u_e C_H$ is the heat transfer coefficient.

For $\dot{m}/\alpha_1 \mu_1 \ll 1$ **, Eqs. (1), (2) and (4) may be combined to give the following expression for the reduction in B'_{eq} due to nonequilibrium effects

$$B' = B'_{\text{eq}} \left[1 - \frac{\dot{m}}{\alpha_1 \mu_1} \right] \quad (7a)$$

For the binary system presently being considered, the \bar{m} in Eq. (6) can be written in terms of \bar{m}_1 , \bar{m}_2 , p_1 and p_e . This expression can then be combined with Eq. (4) to give the following approximate relationship between B' and B'_{eq} for $\sqrt{2\pi RT_w \bar{m}_1} \rho_e u_e C_H / \alpha_1 \bar{m}_2 p_e \ll 1$

$$B' = B'_{\text{eq}} \left\{ \frac{1 - \frac{\sqrt{2\pi RT_w \bar{m}_1} \rho_e u_e C_H}{\alpha_1 \bar{m}_2 p_e}}{1 + B'_{\text{eq}} \frac{\sqrt{2\pi RT_w \bar{m}_1} \rho_e u_e C_H}{\alpha_1 \bar{m}_2 p_e}} \right\} \quad (7b)$$

From Eqs. (7a) and (7b) we see that the nonequilibrium value of the mass addition parameter B' is always less than the equilibrium value B'_{eq} . The degree of departure from equilibrium is proportional to \dot{m}/μ_1 , or $\rho_e u_e C_H / p_e$ and inversely proportional to α_1 . As the net transfer rate of mass between phases increases relative to the rate of mass striking the wall μ_1 , nonequilibrium effects increase. The ratio \dot{m}/μ_1 is proportional to $\rho_e u_e C_H / p_e$ so that maximum nonequilibrium effects will be seen when large heat transfer coefficients occur at low pressures.

Mass Conservation Equation - Multiple Species

The above equations were restricted to a binary system with no surface chemistry other than the vaporization or sublimation process. For graphite ablation, it is necessary to consider multiple carbon species at the wall as well as chemical reaction of the carbon with the free stream gas. Equation (3) for graphite ablation becomes⁽⁶⁾

** Equations (7a) and (7b) are both obtained by expanding in a binomial series and retaining the first two terms.

* For unity value of Lewis and Prandtl numbers

$$B' = \frac{\sum K_{i,w} + F_O + F_N}{1 - \sum K_{i,w} - F_N} \quad (8a)$$

where F_O and F_N result from the carbon-oxygen and carbon-nitrogen chemical reactions, respectively. The mass fractions $K_{i,w}$ now enter as a summation over all carbon species i .

The functions F_O and F_N are given by

$$F_O = \frac{\eta_{C_2}}{\eta_{O_2}} \tilde{K}_{O_2}$$

$$F_N = \left[\frac{\eta_{C_2}}{\eta_{CN}} K_{CN} + \frac{\eta_{C_2}}{\eta_{C_2N_2}} K_{C_2N_2} + \frac{\eta_{C_4}}{\eta_{C_4N_2}} K_{C_4N_2} \right]_w$$

where \tilde{K}_{O_2} for air is 0.232. The carbon-nitrogen compound mass fractions at the wall were presently calculated assuming gas phase chemical equilibrium.* The equilibrium constants were obtained from Dow Chem⁽⁷⁾. The mass fractions, $K_{i,w}$, may again be related to the partial pressures p_i and the molecular weights η_i . So that B' may be written

$$B' = \frac{\sum p_i \eta_i + p_e \bar{\eta} [F_O + F_N]}{p_e \bar{\eta} [1 - F_N] - \sum p_i \eta_i} \quad (8b)$$

Equation (8b) is applicable in general. For the equilibrium case, the p_i 's are given by the individual p_i^v at the wall temperature. For the nonequilibrium case, p_i is determined from Eq. (6) written for each of the i species. It should be noted that for the multiple species case, the $\bar{\eta}$ in Eq. (6) depends on $\sum p_i \eta_i$ so that an iteration procedure is required. The α_i 's used in Eq. (6) were the "nominal values" given by Dolton, et al, i.e., $\alpha_1 = 0.24$, $\alpha_2 = 0.5$, $\alpha_3 = 0.023$, $\alpha_4 = 0.25$ and $\alpha_5 = 0.0019$. All the calculations presented here were obtained using the carbon species thermochemical data of Palmer and Shuler⁴ to calculate p_i for species C_1 through C_5 (see Appendix A).

Energy Conservation Equation

As shown in Fig. 3, the energy conservation equation at the interface can be written

$$\dot{q}_c = \rho_e u_e C_H [H^0 - H_w] - \dot{m} [H_w - H_s] - \epsilon \sigma T_w^4 + \dot{q}_{ext} \quad (9)$$

where \dot{q}_c and \dot{q}_{ext} are the net conduction heat flux into the body and the external radiation heat flux; H^0 , H_w and H_s are the stagnation enthalpy, the enthalpy of the gas at the wall and the enthalpy of the solid at the wall, \dot{m} is the total mass flux of ablating species and $\epsilon \sigma T_w^4$ is the radiation heat flux away from the wall.

* This simplifying assumption is justified by the very small (< 5 percent of total) surface mass loss associated with nitrogen chemistry.

$$\dot{q}_c = \dot{q}_{diff} - \dot{q}_{conv} - \dot{q}_r + \dot{q}_{ext}$$

$$\dot{q}_c = \rho_e u_e C_H [H^0 - H_w] - \dot{m} [H_w - H_s] - \epsilon \sigma T_w^4 + \dot{q}_{ext}$$

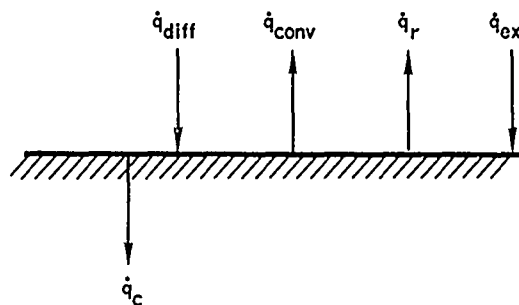


Fig. 3. Macroscopic Surface Energy Balance

Nonequilibrium effects are contained implicitly in the energy equation through effects on the ratio, $\dot{m}/\rho_e u_e C_H$, i.e., B' and on H_w which is evaluated based upon p_i instead of on p_i^v .

Primary Dependent and Independent Variables

Equations (5) or (8) and (9) provide two equations in the primary dependent variables B' and H_w . Solving these equations together satisfies the surface mass and energy conservation equations simultaneously and provides a unique value of B' and H_w . For the equilibrium case both B' and H_w are functions of the edge pressure p_e and the wall temperature T_w . If the steady state ablation assumption is made, i.e., $\dot{q}_c = \dot{m} [H_w - H_b]$, Eq. (9) may be written

$$B' \frac{[H_w - H_b] + H_w}{H^0} + \frac{\epsilon \sigma T_w^4 \frac{C_{H_2O}}{C_H}}{\dot{q}_{cw}} = 1 \quad (10a)$$

where the substitution $\rho_e u_e C_H H^0 = \dot{q}_{cw} (C_H/C_{H_2O})$ has been made. The term H_b is the bulk enthalpy of the solid and \dot{q}_{cw} is the cold wall convective heat flux.

Usually the blowing correction C_H/C_{H_2O} is written as a function of B'^{**} . Thus, functionally Eq. (10a) may be written

$$\frac{F_1(p_e, T_w)}{H^0} + \frac{F_2(p_e, T_w)}{\dot{q}_{cw}} = 1 \quad (10b)$$

Writing the energy balance equation in this way was first suggested by Kendall⁽⁸⁾. Equation (10b) provides valuable insight into the determination of the independent variables. The edge pressure p_e is a primary independent variable. The wall temperature T_w , while an independent variable, is

** All calculations reported in this work were based upon laminar correction to the Stanton number to account for surface blowing effects. The relationship used is⁽¹⁴⁾ $C_H/C_{H_2O} = \ln(1.28B' + 1)/1.28B'$.

implicit; the other variables \dot{q}_{cw} and H^0 are not independent but rather related to one another by Eq. (10b). If the value of B' (and therefore of T_w) is fixed at a given pressure p_e , Eq. (10b) may be written

$$\frac{A}{H^0} + \frac{B}{\dot{q}_{cw}} = 1 \quad (10c)$$

where A and B are constants. Thus, the selected value of B' will be obtained (at the pressure p_e) for all combinations of H^0 and \dot{q}_{cw} satisfying Eq. (10c). A graphical solution procedure based upon this, which allows the determination of B' for given p_e , H^0 and \dot{q}_{cw} using a single graph was given by Rindal, et al⁽⁸⁾. In summation, for the equilibrium case B' may be regarded as a function of p_e , H^0 and \dot{q}_{cw} . For fixed p_e , a given value of B' is obtained for all H^0 and \dot{q}_{cw} satisfying Eq. (10c). This is illustrated in Table 1.

Table 1. Equilibrium B' Values

| p_e (atm) | \dot{q}_{cw} (Btu/ft ² -sec) | H^0 (Btu/lb) | T_w (°K) | B' |
|----------------|--|-------------------|---------------|-------|
| 0.1 | 605 | 100000 | 3281 | 0.420 |
| 0.1 | 647 | 40000 | 3281 | 0.420 |
| 0.1 | 734 | 20000 | 3281 | 0.420 |
| 0.1 | 1000 | 10000 | 3281 | 0.420 |
| 0.1 | 3646 | 5000 | 3281 | 0.420 |
| 0.1 | 13112 | 4400 | 3281 | 0.420 |

For a pressure of 0.1 atmospheres, $B' = 0.420$ for all of the H^0 , \dot{q}_{cw} combinations given since they all satisfy Eq. (10c). Note that the wall temperature is the same for all cases also as required. The independent variables for the nonequilibrium case are discussed in the next section.

Discussion of Results

The Nature of Nonequilibrium Effects

To initially illustrate differences in results calculated using the equilibrium and the nonequilibrium formulation, it is informative to make such a comparison for a series of environmental parameters for which the equilibrium mass addition parameter is a constant. If the previous discussion of dependent and independent variables is recalled, the \dot{q}_{cw} , H^0 conditions in Table 1 all give a value of B' (equilibrium assumption) of 0.420. Therefore, let us compare nonequilibrium calculated results with the equilibrium results in

Table 1. These comparisons are shown in Fig. 4. The calculated equilibrium results are all given by the single point indicated by an X on the equilibrium B' curve. Calculated nonequilibrium results have a B' less than the equilibrium value and a wall temperature greater than when solid-gas equilibrium is assumed. The reduction in B' , caused by p_i being less than p_i^* [see Eq. (6)], reaches a reasonably constant value. However, the surface temperature continues to increase over its equilibrium value as H^0 is decreased and \dot{q}_{cw} increases, i.e., as $p_e u_e C_H$ increases. For the equilibrium case, the independent variables were shown to be p_e and all combinations of \dot{q}_{cw} and H^0 satisfying Eq. (10c). From Fig. 4 we see that for the nonequilibrium case, p_e , H^0 and \dot{q}_{cw} are all independent variables by themselves.

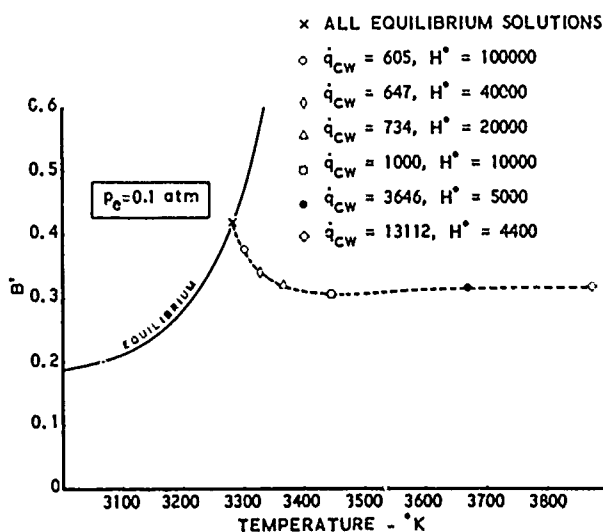


Fig. 4. Differences Between Equilibrium and Nonequilibrium Solutions

Graphical Solution Procedure

All solutions for the equilibrium case can be represented on a single graph using the method of Rindal, et al⁽⁸⁾. However, since there are three independent variables in the nonequilibrium case, there is no convenient way of representing all solutions on a single graph. For a given pressure p_e there is a unique value of B' and T_w for specified H^0 and \dot{q}_{cw} as shown in Fig. 4. This suggests that for given p_e , a convenient way of graphically presenting results would be to plot lines of constant H^0 and constant \dot{q}_{cw} in the same B' , T_w plane as in Fig. 4. Such a plot for an edge pressure, p_e , of one atmosphere is shown in Fig. 5. For this pressure, Fig. 5 gives B' values and surface temperature for \dot{q}_{cw} ranging from 2000 to 15000 Btu/ft²-sec and for the H^0 values of 5000 to 50000 Btu/lb. Such a plot would be very useful for instance for graphite arc jet ablation results at constant pressure where the stagnation enthalpy H^0 and the cold wall heat flux \dot{q}_{cw} are varied by changing the arc current and the body geometry.

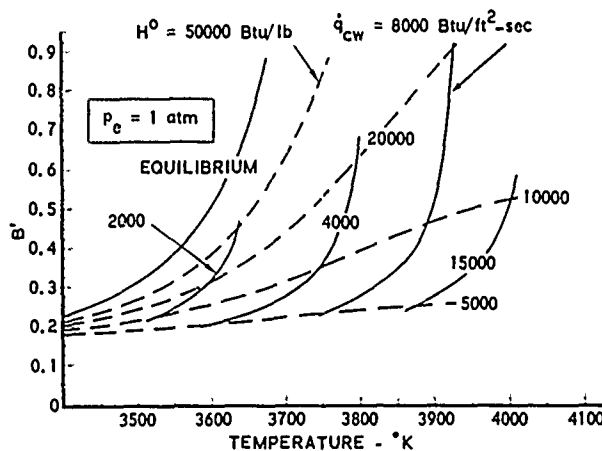


Fig. 5. Nonequilibrium Effects on B' and T_w

Mass Loss and Surface Temperature Differences for Typical Reentry Vehicle Environments

Nonequilibrium calculations have been shown to result in lower values of B' and larger wall temperatures. The surface recession rate \dot{s} is obtained from B' through the relationship

$$\rho_b \dot{s} = B' \dot{q}_{cw} \left(\frac{C_H}{C_{H_0}} \right)$$

where ρ_b is the bulk density of the ablating material. Quantitative results showing the differences in the calculated surface recession rate \dot{s} and the surface temperature T_w for a wide range of reentry environments are shown in Figs. 6 and 7. For stagnation enthalpies of 2000, 5000 and 10000 Btu/lb, pressures from 0.1 to 100 atmospheres and cold wall heating values from 300 to 75000 Btu/ft²-sec, Fig. 6 shows that the difference in the calculated recession rate due to the equilibrium assumption is never greater than 30 percent. The corresponding differences in the surface temperature, shown in Fig. 7, range up to a maximum of about 600°K obtained when the equilibrium surface temperature is predicted to be about 3400°K, whereas the calculated nonequilibrium temperature is about 4000°K. In both Figs. 6 and 7 we see that the largest differences occur at lower pressures (with larger $\rho_b u_e C_H$) where the ratio of the interphase mass transfer rate to the collision frequency at the wall is largest. These differences are of the same order as those due to the assumption of alternate carbon species thermochemistry models⁽⁹⁾. Since over 90 percent of the total recession occurs at pressures greater than 10 atmospheres for typical reentry trajectories, it can be seen from Fig. 6 that the difference in the total integrated recession will be the order of 5 to 10 percent maximum. Thus the added complexity of the nonequilibrium formulation is not justified for reentry vehicle nosetip surface recession predictions. However, a 600°K difference in the surface temperature may not be tolerable for thermostructural design purposes.

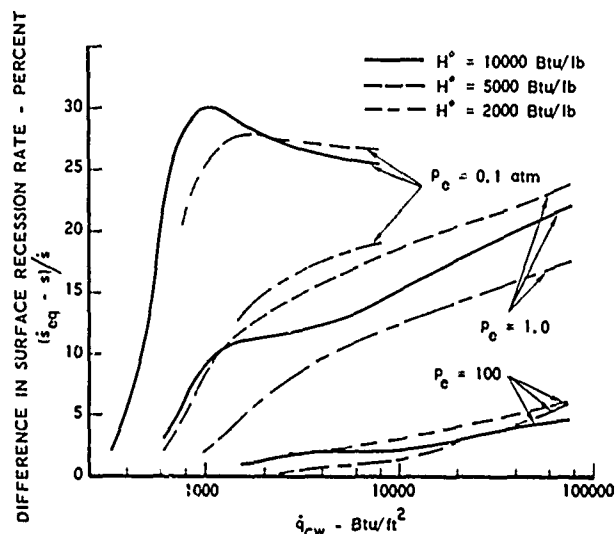


Fig. 6. Nonequilibrium Effect on Surface Recession Rate

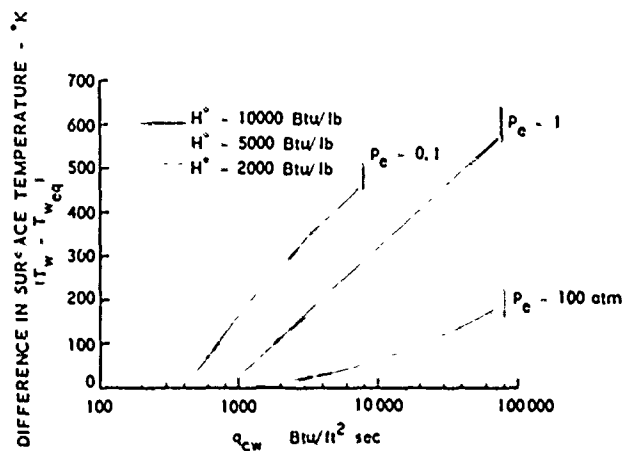


Fig. 7. Nonequilibrium Effect on Surface Temperature

Graphite Melt Considerations

The question of whether graphite will melt under reentry vehicle convective heating environments has been considered by Rindal and Powers⁽¹⁶⁾ and by Kratsch⁽¹⁰⁾. These authors conclude that for high beta reentry vehicle trajectories it is possible, for small nose radii, (1/4 to 1/2 in.) to reach an assumed melt temperature in the range of 4000 to 4200°K.

The equations described in this work are applicable up until the time that the wall temperature reaches the melt temperature. When the melt temperature is reached, additional modeling of the melt layer on the surface is required. Equilibrium and nonequilibrium calculations were performed to determine differences in the heat

flux required to reach an incipient melt temperature of 4200°K at a pressure of 100 atmospheres for stagnation enthalpies of 2000, 5000 and 10000 Btu/lb. For $H^0 = 10000$ Btu/lb, the required heat flux values from the equilibrium and nonequilibrium formulations were 3000 and 2750 Btu/ft²-sec, respectively. For $H^0 = 5000$ Btu/lb, the corresponding required heat flux values were 21700 and 6700 Btu/ft²-sec. Thus melting could occur at this stagnation enthalpy based upon the nonequilibrium calculation. However, the required equilibrium value of \dot{q}_{cw} is over 300 percent larger and could not be obtained at this enthalpy.

A melt temperature for graphite in the range 4000-4200°K is not universally accepted. There is some old⁽¹¹⁾ as well as some very recent⁽¹²⁾ evidence that the melt temperature is about 3800°K and that the triple point pressure is closer to 1 atmosphere than to 100 atmospheres. Therefore, calculations like those above were made for an incipient melt temperature of 3800°K for pressures ranging from 10 to 100 atmospheres. The results are shown in Fig. 8. The difference in the calculated heat flux required to attain incipient surface melting is quite small over the whole range of pressure for $H^0 = 10000$ Btu/lb. For $H^0 = 5000$ Btu/lb, the equilibrium prediction for heat flux is 50 percent too high at lower pressures. For ground test environments with stagnation enthalpies in the range 2000-5000 Btu/lb, differences of over 200 percent can occur even at a pressure of 100 atmospheres.

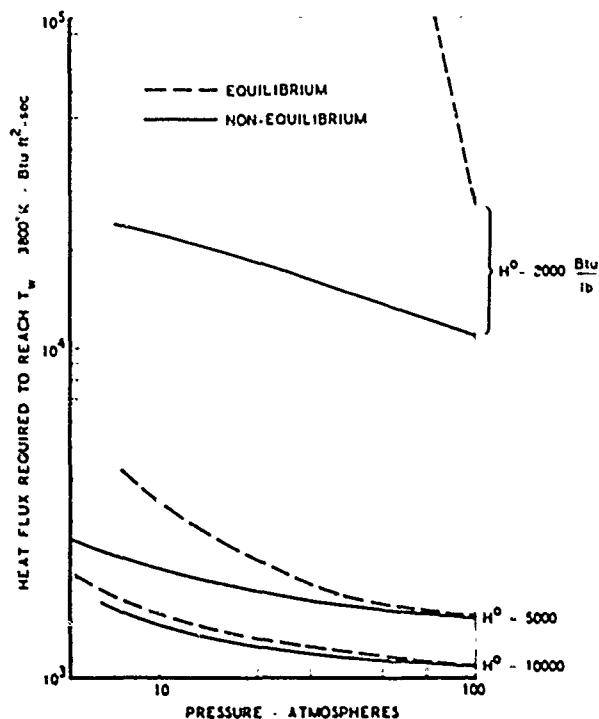


Fig. 8. Nonequilibrium Effects on Melt Temperature Environments

I am indebted to Dr. A. G. Whittaker for bringing this reference to my attention.

These results indicate very large differences in the predicted heating environment required to reach incipient melt conditions can occur when the solid-gas equilibrium assumption is made. Once the melt temperature is reached, the liquid graphite has a vaporization rate (B') much greater than the solid graphite^(10, 11). Because of this, essentially 100 percent of the liquid melt layer is vaporized and very little is stripped off as liquid. Thus, nearly full advantage may still be taken of the very large amount of heat required to change solid graphite to gaseous species in the boundary layer. However, when the surface temperature has reached the melt temperature, the modeling must be changed to account for the presence of liquid graphite as done by Kratsch⁽¹⁰⁾. No attempt was made to carry out this type of modeling in the present work.

Radiation Heating Effects

Results presented thus far have been restricted to a convective heating environment for ground test or flight applications. If the free stream velocity is increased from reentry vehicle values like 25000 ft/sec to superorbital velocities like 50000 ft/sec, gas cap radiation heating to the solid surface becomes important in addition to the convective heating. Graphite ablation predictions for an Apollo type vehicle reentering the earth's atmosphere at superorbital velocities have been made by Bartlett, et al⁽¹³⁾.

Equilibrium and nonequilibrium calculations were made for the range of convective and radiation heating levels given⁽¹³⁾. The particular conditions chosen were an altitude of 220000 ft and a velocity of 45000 ft/sec which result in a stagnation pressure of 0.23 atmosphere and a stagnation enthalpy of 40318 Btu/lb. The calculated results are summarized in Table 2. The surface temperature difference is quite small over the whole range of conditions. The surface recession rate difference is small until the condition of low convective heating rate and higher radiation heating rate associated with larger nose radius is approached. For these heating conditions the calculated B'_{eq} may be nearly twice the nonequilibrium value, with both B' and B'_{eq} becoming significantly greater than one, i.e., massive blowing. Despite the large difference in B' , the difference in the predicted recession rate \dot{s} is only about 25 percent because of a compensating effect associated with the blowing correction to the convective heating rate. Thus, there appears to be no substantial differences in either the wall temperature or the surface recession rate for superorbital reentry conditions.

The above statement regarding differences depends intimately upon the validity of the blowing correction to the convective heat transfer rate in a radiation augmented heating environment where B' is being driven to very large values by the external radiation heating. This type of coupling was not present in the data upon which present blowing corrections are based. It would thus be desirable to obtain new data in which B' is very large due to external radiation heating. In Table 3, calculated

When the equilibrium B' is much larger than the nonequilibrium B' , C_H/C_{H_0} is much less for the equilibrium case. Since $\rho_b \dot{s} = B' \dot{q}_{cw} C_H/C_{H_0}$, the two effects compensate.

Table 2. Superorbital Reentry Calculations

| P_e (atm) | H^0 (Btu/lb) | \dot{q}_{cw} (Btu/r ² -sec) | \dot{q}_{ext} (Btu/r ² -sec) | $T_{w,eq} - T_w$ (°K) | B' | $\frac{B'_{eq} - B'}{B'}$ | $\frac{\dot{q}_{eq} - \dot{q}}{\dot{q}}$ |
|----------------|-------------------|---|--|--------------------------|------|---------------------------|--|
| 0.23 | 40318 | 2503 | 106 | 157 | 1.98 | 0.232 | 0.122 |
| 0.23 | 40318 | 1823 | 166 | 125 | 1.70 | 0.225 | 0.124 |
| 0.23 | 40318 | 1191 | 290 | 88 | 1.44 | 0.220 | 0.128 |
| 0.23 | 40318 | 851 | 426 | 67 | 1.41 | 0.222 | 0.130 |
| 0.23 | 40318 | 596 | 585 | 51 | 1.64 | 0.236 | 0.131 |
| 0.23 | 40318 | 356 | 825 | 41 | 3.32 | 0.338 | 0.146 |
| 0.23 | 40318 | 237 | 975 | 42 | 9.88 | 0.746 | 0.201 |

Table 3. Large B' in a Ground Test Environment

| P_e (atm) | H^0 (Btu/lb) | \dot{q}_{cw} (Btu/r ² -sec) | \dot{q}_{ext} (Btu/r ² -sec) | $T_{w,eq} - T_w$ (°K) | B' | $\frac{B'_{eq} - B'}{B'}$ | $\frac{\dot{q}_{eq} - \dot{q}}{\dot{q}}$ |
|----------------|-------------------|---|--|--------------------------|------|---------------------------|--|
| 0.32 | 4698 | 705 | 1735 | 181 | 0.86 | 0.320 | 0.209 |
| 0.32 | 4698 | 705 | 2193 | 194 | 1.18 | 0.341 | 0.203 |
| 0.32 | 4698 | 705 | 3000 | 213 | 1.94 | 0.399 | 0.196 |
| 0.32 | 4698 | 705 | 5000 | 256 | 5.64 | 0.578 | 0.193 |
| 0.32 | 4698 | 705 | 6000 | 278 | 16.0 | 0.809 | 0.221 |

*Conditions in experiments of Wakefield¹⁴
 †Increased \dot{q}_{ext} above Reference 14 values

B' and B'_{eq} values for several radiation heating levels at and above those in the ground test experiments of Wakefield¹⁴ are tabulated. From this we see that questions regarding the validity of present blowing corrections to the convective heating rate in highly coupled radiation-convective heating environments could be explored by conducting new ground tests with radiation levels 2 to 3 times higher than those in Wakefield's experiments.

Summary and Conclusions

Comparison of equilibrium and nonequilibrium calculated results for the same environmental conditions indicates that the mass addition parameter, B' , is always less and the wall temperature is always greater for the nonequilibrium case. For a given pressure, the difference in B' levels off and the difference in wall temperature continues to increase as \dot{q}_{cw} increases and H^0 decreases, i.e., as the heat transfer coefficient increases.

For the nonequilibrium case, p_e , H^0 and \dot{q}_{cw} are all independent variables. A convenient

graphical solution procedure for a given pressure is to plot lines of constant stagnation enthalpy H^0 and lines of constant cold wall heat flux \dot{q}_{cw} in the B' , T_w plane.

Comparison of calculated equilibrium and non-equilibrium results for a wide range of reentry vehicle environmental conditions indicates a maximum difference in the calculated recession rate of 30 percent and a maximum difference in the surface temperature of 600°K. The largest differences occur at low pressures for large heat transfer coefficients.

If the graphite melt temperature is 3800°K, then nonequilibrium calculations should be used to determine the heat flux required for incipient melting for stagnation enthalpies less than 5000 Btu/lb since differences as large as 200 to 300 percent can occur.

Radiation augmenting of the convective heating environment can cause a dramatic increase in B' . When this happens differences in B' of over 100 percent can occur. However, the corresponding difference in the surface recession rate is only about 25 percent. This effect occurs for super-orbital reentry velocity conditions when the convective heating rate is low and the radiation heating rate is high, i.e., for large nose radii. Ground test simulation of this effect is possible by increasing the external radiation level of the experiments of Wakefield 2 to 3 times. In this way, experimental determination of the validity of the blowing correction, CH/CH_0 , could be made for a coupled convective-radiation heating environment at the very high B' values of interest.

Appendix: Thermochemistry Data

All of the calculations presented here were obtained using the carbon species C_1 through C_5 thermochemical data of Palmer and Sheref⁽⁴⁾. The values used were termed in that very extensive survey paper the "approximate best." Putting the carbon species vapor pressure equations in the form

$$\ln p_1^v \text{ (atm)} = \frac{A}{T(^{\circ}\text{K})} + B \quad (\text{A-1})$$

the Palmer and Sheref values of A and B ⁽¹⁵⁾ are tabulated in Table A-1.

Table A-1. Constants from Palmer and Sheref

| A | B |
|---------|-------|
| - 85715 | 18.69 |
| - 98363 | 22.20 |
| - 93227 | 23.93 |
| -150307 | 31.30 |
| -133087 | 32.71 |

References

1. Dolton, J. A., R. E. Mauer and H. E. Goldstein, "Thermodynamic Performance of Carbon in Hyperthermal Environments," AIAA Paper No. 68-754, AIAA Third Thermophysics Conference, Los Angeles, California, June 1968.
2. Kratsch, K. M., M. R. Martinez, F. I. Clayton, R. B. Greene, and J. E. Wuerer, "Graphite Ablation in High Pressure Environments," Douglas Paper 5162, Presented to AIAA Entry Vehicle Systems and Technology Conference, Williamsburg, Virginia, December 1968.
3. Lundell, J. H. and R. R. Dickey, "Graphite Ablation at High Temperatures," AIAA Paper No. 71-418, AIAA Sixth Thermophysics Conference, Tullahoma, Tennessee, April 1971.
4. Palmer, H. B. and Mordecai Shelef, "Vaporization of Carbon," Chemistry and Physics of Carbon, 4, Marcel Dekker, Inc., New York, 1968.
5. Kubota, T., "Ablation with Ice Model at M=5.8," ARS Journal, pp. 1164-1169, December 1960.
6. Lees, L., "Convective Heat Transfer with Mass Addition and Chemical Reactions," Combustion and Propulsion, Third AGARD Colloquium, pp. 451-498, Pergamon Press, 1959.
7. JANAF Thermochemical Tables, The Dow Chemical Company, Midland, Michigan, 1969.
8. Rindal, R. A., T. J. Dahm, and D. F. McVey, "Graphite Temperature and Ablation Characteristics in Various Environments," AIAA Paper 69-148, January 1969.
9. Rindal, R. A. and C. A. Powars, "Effects of Carbon Vapor Thermochemistry Uncertainties on R/V Ablation Predictions," AIAA Paper No. 71-414, AIAA Sixth Thermophysics Conference, Tullahoma, Tennessee, April 1971.
10. Kratsch, K. M., "Graphite Fusion and Vaporization," Douglas Paper 5338, Presented to ASME/AIAA Tenth Structures, Structural Dynamics and Materials Conference, New Orleans, Louisiana, April 1969.
11. Konig, Hans, "The Melting of Carbon," Naturwissenschaften, 34, pp. 108-111, 1947.
12. Whittaker, A. G. and P. L. Kintner, "Laser-Heating Studies of Carbon Melting and Vaporization," Presented at American Ceramic Society 27th Pacific Coast Regional Meeting, North Hollywood, California, 23-26 October 1974.
13. Barlett, E. P., W. E. Nicolet and J. T. Howe, "Heat-Shield Ablation at Supersonic Reentry Velocities," Journal of Spacecrafts and Rockets, 8(5), pp. 456-463, May 1971.
14. Wakefield, R. M. and D. L. Peterson, "A Study of Graphite Ablation in Combined Convective and Radiative Heating," AIAA Paper No. 72-88, January 1972.
15. Palmer, H. B., Pennsylvania State University, University Park, Pennsylvania, Personal Communication.
16. Rindal, R. A., "Thermochemical and Thermomechanical Ablation," Appendix D of AFML TR 69-73, Vol. IV, January 1970.